Journal of Power Sources 246 (2014) 149–159

Contents lists available at SciVerse ScienceDirect

Journal of Power Sources

journal homepage: www.elsevier.com/locate/jpowsour

Modeling the delamination of amorphous-silicon thin film anode for lithium-ion battery

Siladitya Pal [a], Sameer S. Damle [b,e], Siddharth H. Patel [c], Moni K. Datta [a,e], Prashant N. Kumta [a,b,d,e], Spandan Maiti [a,b,e,*]

[a] Department of Bioengineering, University of Pittsburgh, PA 15261, USA
[b] Department of Chemical Engineering, University of Pittsburgh, PA 15261, USA
[c] Department of Mechanical Engineering, Michigan Technological University, MI 49931, USA
[d] Mechanical Engineering and Materials Science, University of Pittsburgh, PA 15261, USA
[e] Center for Complex Engineered Multifunctional Materials, University of Pittsburgh, PA 15261, USA

HIGHLIGHTS

- Computational study of electrochemical cycling induced film delamination has been undertaken.
- Current collector mechanical properties significantly influence cycling response.
- Elasto-plastic current collectors show partial delamination of the thin film.
- Absence of interfacial delamination in thin Si film on low modulus elastic substrate.

ARTICLE INFO

Article history:
Received 4 January 2013
Received in revised form
13 June 2013
Accepted 14 June 2013
Available online 25 June 2013

Keywords:
Li-ion battery
a-Si thin film anode
Diffusion induced stress (DIS)
Interfacial delamination
Current collector
Mechanical properties

ABSTRACT

Sputter-deposited amorphous silicon thin films on metallic copper current collectors are widely studied as lithium-ion anode systems. Electrochemical results indicate these electrodes exhibit near theoretical capacity for first few cycles; however delamination at the thin film–current collector interface causes rapid capacity fade leading to poor cycling performance. Primary reason for this interfacial delamination is the mechanical stress generated due to colossal volume expansion of silicon during lithiation. The focus of the current study is to present a mechanistic understanding of the role of mechanical properties of the current collector on this characteristic delamination behavior during electrochemical cycling. Toward this end, we have developed a computational framework that accounts for the coupled diffusion induced large deformation in silicon, elasto-plastic deformation of the current collector, as well as the nucleation and propagation of interfacial delamination. We have also performed a detailed parametric study to investigate the effect of mechanical properties of the current collector on the delamination of the thin film–current collector interface. We have accordingly determined that current collectors with low elastic modulus such as graphite can completely suppress interfacial delamination. Our analysis thus provides a sound mechanistic approach for designing next generation Si thin film anodes with improved capacity retention.

1. Introduction

Lithium-ion batteries (LIBs) at present are widely considered as the flagship energy storage system for a variety of portable consumer electronic devices and transportation systems. Sony introduced first commercial LIB based on $LiCoO_2$ and carbon anode in 1991 to be used primarily in portable consumer electronic devices. Since then, the LIB system and the area in general, has witnessed tremendous research activity focused at primarily improving the capacity and cycling performance to support the increasing energy storage demands of new and emerging portable and consumer electronic devices, while extending its application to transportation systems. Accordingly, the application of LIBs today extends exclusively not only to laptops, camcorders and cameras but also to smart cellular phones, hybrid and plug-in electric vehicles (HEV's, PHEVs), all electric vehicles (EVs), as well as several advanced aerospace applications. The current universally accepted energy

* Corresponding author. Department of Bioengineering, University of Pittsburgh, Pittsburgh PA 15261, USA. Tel.: +1 412 624 4240; fax: +1 412 383 8788.
E-mail address: spm54@pitt.edu (S. Maiti).

0378-7753/$ – see front matter © 2013 Elsevier B.V. All rights reserved.
http://dx.doi.org/10.1016/j.jpowsour.2013.06.089

storage system status shared by LIBs is a consequence of intense research directed particularly in the cathode area, although over the last few years since the mid 2000 there has been a conscious effort directed at developing new anodes and improved electrolytes. Despite this, graphite is still the preferred and commercially used anode material in LIBs to date exhibiting a theoretical capacity of 372 mAh g^{-1}.

With the growing energy storage demands and continued miniaturization of advanced portable and consumer systems, there is a stringent need for longer lasting portable energy storage systems with high energy and power densities. Thus with identification and improvements in the cathode area, there is a need for the development of new anodes. In this respect, silicon based anodes have emerged as the front runner due to its very high specific capacity (3580 mAh g^{-1}). However, silicon undergoes colossal volume expansion during lithiation ($\sim$300%), and the diffusion-induced stresses result in the formation of cracks with deleterious effects on the battery performance. Furthermore, as is known, the volumetric expansion related stresses result in delamination of silicon from the current collectors leading to loss of electrical contact causing poor cycling performance of this particular configuration [1]. To improve the mechanical integrity during electrochemical cycling and thus help retain the capacity, various silicon based anode configurations in the form of nanotubes, nanowires, core shell structures, single/multi layer thin films, patterned nanostructures, etc. have been synthesized and tested for their electrochemical performance in LIB [2–4]. Amorphous silicon based thin film anodes in particular have shown potential to be the next-generation anodes due to their near-theoretical performance of 3580 mAh g^{-1} and reduced influence of volumetric stress related catastrophic failure due to the available free volume for accommodation of the stresses [5].

1.1. Mechanical properties of the interface: a vital parameter

Mechanical integrity of the thin film–current collector interface and hence the performance of *a*-Si thin film anode depends on the mechanical properties of the interface and the current collector, as well as the geometric factors such as thin film dimensions. Modification of the substrate surface morphology to increase the adhesion of *a*-Si thin film with the substrate has shown to improve the cycling performance [6]. Annealing the *a*-Si thin film deposited on Cu substrate at high temperature is also known to improve the adhesion between the two surfaces by interdiffusion of Si and Cu [7]. Thus, it has been reported that better attachment of thin film with the substrate delays the interfacial crack propagation resulting in lower capacity fade. Recently, patterning of the thin film has garnered attention as a possible avenue to mitigate delamination at the interface [8–10]. In a series of papers, Gao and coworkers have theoretically studied the effect of size of thin film islands on interfacial delamination [11–14]. They have determined the existence of a critical size of the islands, below which delamination will not occur and further propagate. Another strategy to suppress delamination that has not garnered much attention yet is the proper choice of current collector and its mechanical properties to safely accommodate the stresses generated during electrochemical cycling of the anode. Recent experiments show that the presence of an interfacial layer of amorphous carbon between *a*-Si thin film and substrate results in excellent capacity retention of the thin film anode [15]. Motivated by this observation, we present for the first time a systematic study of the effect of mechanical behavior of the current collector on the onset and propagation of the interfacial delamination of the thin film anode. We selected elastic modulus and yield strength as the two essential mechanical properties to effectively categorize the performance of the candidate current collector materials. In doing so, the goal is to provide and identify candidate current collector systems that will be conducive for effectively mitigating the deleterious effects of the catastrophic failure in Si.

We accordingly present herein a thermodynamically consistent theoretical framework that considers the large deformation as well as failure response of the anode materials system coupled with the necessary voltage performance of the electrode. We demonstrate predictive capability of the presented model through the simulation of voltage–capacity curves for a thin film configuration subjected to different charge rates. Also, our model can simulate the interfacial crack propagation leading to capacity fade and ultimate failure of the anode. We postulate that a process zone precedes the actual nucleation of a crack, and thus can be modeled using the cohesive zone technique. The presented model includes elastic as well as elasto-plastic behavior of the underlying current collector, and thus can examine the interaction of its passive mechanical response with the active response of *a*-Si. Utilizing this model, we demonstrate the effect of substrate mechanical properties on the delamination of the thin film from the current collector.

The paper is organized into various sections: In Section 2, we detail our modeling framework with an emphasis on initiation and propagation of interfacial delamination. Experimental methods to determine open circuit voltage to be used in our simulation are presented in Section 3 along with the details of the numerical model. The model is validated in Section 4 against experimental voltage–capacity response of a representative thin film anode based half cell. We further demonstrate the predictive capability of our model by simulating the same response for different charge rates, and contrast our findings with experimental ones. We also present a detailed parametric study of interfacial delamination by systematically varying mechanical properties of the current collector. We discuss the simulation results and their implications on the design of thin film anode in Section 5. We compare our findings with experimental results wherever possible. We finally conclude the article by summarizing the merits of the different current collector materials with potential suggestions for future improvements.

2. Model description

Recently a few models have appeared in the literature [16–20] that have focused on coupled diffusion and stress generation in the large deformation regime. Crack propagation in a cylindrical graphite particle [21] as well as in a silicon nanowire due to diffusion induced stress has also been studied [22]. However, the present modeling framework focuses particularly on interfacial delamination of thin film anode from the current collector rather than its bulk disintegration, which is a critical factor affecting the thin film Si anode failure. Importance of this mode of failure on the cyclic performance of thin film based anodes has been studied experimentally by our group a few years ago in the work reported by Maranchi et al. [1]. Possible mechanisms for such failures have also been discussed recently through theoretical considerations [8,11–14]. We complement these research efforts by presenting an experimentally validated comprehensive computational framework that will enable us to investigate the interplay between various electrochemical and mechanical phenomena responsible for delamination of the thin film–current collector interface. The present model hence seamlessly integrates electrochemical charge/discharge cycling with stress-assisted delamination of silicon thin film anode from current collector (see Fig. 1(a)). The Faradaic reaction at the anode/electrolyte interface is modeled using the classical Butler–Volmer approach. Lithium atom (reduced state) further diffuses into the bulk of the anode that undergoes large volume expansion, in turn generating large stresses. A detailed thermodynamically consistent framework

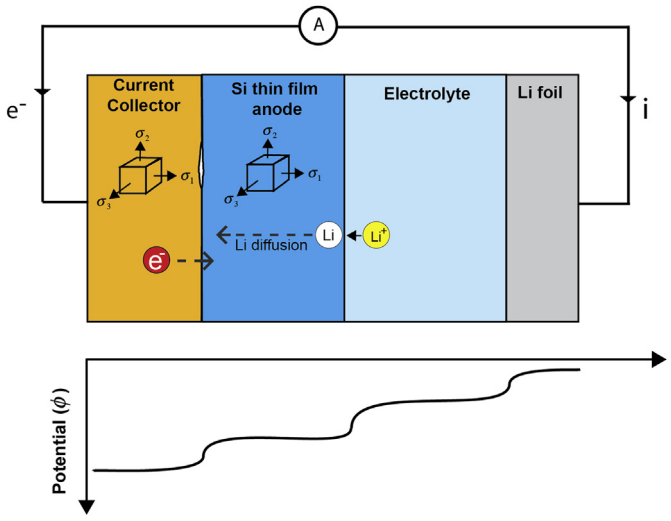

Fig. 1. (a) Schematic representation of the half-cell consisting of current collector, Si thin film anode, electrolyte and the Li foil counter electrode. Partial delamination at thin film–current collector interface is also indicated. (b) Variation of potential at different interfaces within the half-cell.

for the anode material has been developed coupling transport of lithium and large deformation of bulk silicon. We assume that the generated volumetric stress does not affect the redox reaction at the anode/electrolyte interface. The current collector that provides the electronic path for redox reaction also undergoes deformation as it is attached to the anode as demonstrated by Maranchi et al. [1]. Our model thus incorporates possible elasto-plastic deformation of this material in the large deformation regime. We also model the nucleation and propagation of cracks at the interface of thin film and current collector through a cohesive zone approach. Salient components of our modeling framework will be detailed in the next sections.

2.1. Electrochemical reaction kinetics at the electrolyte–Si thin film interface

Electrochemical reaction takes place at the interface of the electrolyte and silicon anode, as seen in Fig. 1(a). We consider a Faradaic reaction only at the flat electrode surface where lithium atom Li^+ is reduced by an electron e^- to produce lithium atom as $Li^+ + e^- \rightleftharpoons Li$. Net reaction rate at the interface is the difference between the oxidation and reduction reaction rate. When both the rates are equal, the potential difference measured across the half-cell depends on the state of charge ($\bar{x}$) of the anode and is known as the open circuit potential $U_{OCP}(\bar{x})$. The departure from the state of equilibrium due to application of an external potential source is expressed by overpotential and is defined as $\eta_s = V - U_{OCP}(\bar{x})$. Negative value of overpotential is indicative of cathodic current (lithiation) while positive value signifies anodic current (delithiation). When the diffusion resistance in the electrolyte can be neglected, the charge transfer reaction kinetics, i.e., the relation between the current i with the over-potential η_s at the electrode–electrolyte interface is given by the well known Butler–Volmer equation as Ref. [23]

$$i = i_0\left[\exp\left(\frac{\alpha_a F}{RT}\eta_s\right) - \exp\left(\frac{-\alpha_c F}{RT}\eta_s\right)\right] \quad (1)$$

where the exchange current density is $i_0 = Fk(c_e)^{\alpha_a}(c_{max} - c_s)^{\alpha_a}(c_s)^{\alpha_c}$. Exchange current density at the anode surface depends on the surface concentration of Li in the anode material c_s and its maximum value c_{max}, and Li ion concentration in the electrolyte c_e with a reaction rate constant of k. The anodic and cathodic transfer coefficients are denoted as α_a and α_c, respectively. Values of k depend on the type of reaction (lithiation/delithiation) occurring at the anode.

The voltage diagram in Fig. 1(b) shows the voltage drop across the electrode. Delamination of the electrode material from the current collector hinders the conduction of electron between these two domains and manifests itself as an additional voltage drop reducing the available potential from a net reduction or oxidation reaction. This potential drop can be estimated as an Ohmic drop arising from an increase in contact resistance R_c associated with the interfacial area A_c between the current collector and thin film. Resultant potential difference across half-cell in such a case is obtained as $V = U_{OCP}(\bar{x}) + \eta_s + \Delta\varphi_{oh}$. The Ohmic drop contributed by the charge/discharge current, i passing through the interface between the current collector and silicon thin film is given by $\Delta\varphi_{oh} = (R_c/A_c)i$. In this expression, A_c represents the interfacial area, while the contact resistance is denoted by R_c. Evidently, when the contact area reduces to zero, i.e., delamination of the silicon thin film from the current collector is complete, Ohmic drop becomes infinity rendering the cycling of the electrochemical cell infeasible.

In the present study, galvanostatic electrochemical charge/discharge cycling of Si anode is considered. Therefore the total current i supplied or drawn from anode is known for the entire electrochemical cycle and depends on the C-rate. As a constant current is drawn or supplied to the anode, the rate of Li^+ reduction at the interface is constant and is related to the current through Faraday's law. Thus lithium flux at the boundary of the anode is given as $J_{Li} = i/F$.

In order to determine over-potential from the Butler–Volmer equation, value of equilibrium potential $U_{OCP}(\bar{x})$ at a given state of charge is required. For higher fidelity of the predictions from our model, this quantity has been experimentally determined by Galvanostatic Intermittent Titration Technique (GITT) [24] using a similar thin film anode configuration that has been used for the simulation purpose. Details of this experimental technique have been furnished in Section 3.1.

2.2. Li transport in Si thin film and associated mechanical deformation

During electrochemical cycling of the half-cell, Li atoms are transported through the bulk of the silicon anode. However, this phenomenon induces large volume expansion and associated mechanical stress, and this in turn influences the transport of lithium. We present a model to include these two strongly coupled phenomena in the premise of large deformation mechanics and non-equilibrium thermodynamics.

To account for large deformation of the silicon domain due to the lithiation reaction, a multiplicative decomposition of the total deformation gradient of the form $\boldsymbol{F} = \boldsymbol{F}_e\boldsymbol{F}_\theta$ has been considered. In this expression, $\boldsymbol{F}_\theta$ denotes the component of the deformation gradient arising from the intercalation, $\boldsymbol{F}_e$ denotes deformation coming solely from elastic deformations. Details of the mathematical model development are presented in Supplementary Information (SI) material (see Fig. S1) as well as in Ref. [18]. Fig. S1(b) shows the intermediate (stress free) and final configurations along with deformation gradients. Therefore, the deformation gradient solely due to insertion of lithium in the anode material at zero stress is considered as $\boldsymbol{F}_\theta = (1 + \eta_c)^{1/3}\boldsymbol{I}$, with $\boldsymbol{I}$ being the identity tensor, $c(\boldsymbol{X},t)$ the concentration of the lithium atom in the reference configuration, and η the expansion coefficient assuming isotropic volume expansion.

To obtain the concentration field of lithium during its transport in silicon, we consider the mass conservation of lithium in the reference configuration as

$$\partial_t c + \nabla_X \cdot \boldsymbol{J} = 0 \tag{2}$$

where $\boldsymbol{J}$ is the flux of lithium at a material point $\boldsymbol{X}(t)$. Initial and boundary conditions for lithiation in the anode can be described as

$$c(\boldsymbol{X},0) = c_0(\boldsymbol{X}) \text{ on } \partial\Omega_{0c}, \text{ and } \boldsymbol{J}\cdot\boldsymbol{N} = J_{\mathrm{Li}} \text{ on } \partial\Omega_{0J} \tag{3}$$

with $c_0(\boldsymbol{X})$as the initial concentration of lithium in the anode, J_{Li} as the flux of lithium atom at point $\boldsymbol{X}$ on the electrolyte–anode interface $\partial\Omega_{0J}$ with normal $\boldsymbol{N}$. Diffusion of lithium occurs at a much slower time scale; hence, mechanical equilibrium is assumed to be already achieved. Therefore, the balance of linear momentum can be expressed as:

$$\nabla_X \cdot \boldsymbol{P} = 0 \text{ with } \boldsymbol{P} = \boldsymbol{FS} \tag{4}$$

where, $\boldsymbol{P}$ and $\boldsymbol{S}$ are the first and second Piola–Kirchhoff stress tensors, respectively. The boundary conditions for mechanical equilibrium are given as $\boldsymbol{PN} = \boldsymbol{t}$ on $\partial\Omega_{0t}$, and $\boldsymbol{u} = \boldsymbol{u}_0$ on $\partial\Omega_{0u}$.

An additive decomposition of the free energy functional ψ of the anode material is considered here as:

$$\psi(\boldsymbol{F},c) = \psi_e(\boldsymbol{F}_e,c) + \psi_c(c) \tag{5}$$

with an elastic free energy density ψ_e and chemical free energy density ψ_c. The elastic free energy depends on $\boldsymbol{F}_e$, which further depends on the overall deformation gradient $\boldsymbol{F}$ as well as the concentration of the lithium. Recent findings illustrate that the elastic moduli of crystalline as well as amorphous-Si reduces upon lithiation [25]. To account for such effects, we have considered additional dependence on lithium concentration in the elastic free energy functional $\psi_e(\boldsymbol{F}_e,c)$. However, the chemical energy density of the anode material $\psi_c(c)$ relies solely upon the concentration of lithium. To evaluate the chemical potential and mechanical stresses from this energy functional, we apply thermodynamic principles as detailed in SI (Section 1).

In the present analysis, the atomic flux is derived as

$$\boldsymbol{J} = -D\left[\nabla c - \frac{\eta c}{RT}\nabla S_m + \frac{c}{RT}\nabla\left(\frac{\partial\psi_e}{\partial c}\right)\right] \tag{6}$$

with D as the diffusivity of lithium atom in the anode material. In this equation, S_m is a pressure like quantity defined in SI. Substituting above derived expression for Li flux, mass conservation of Li in the anode material (Eq. (2)) can be expressed as:

$$\partial_t c = D\nabla\left[\nabla c - \frac{\eta c}{RT}\nabla S_m + \frac{c}{RT}\nabla\left(\frac{\partial\psi_e}{\partial c}\right)\right] \tag{7}$$

This equation suggests that the transport of lithium in the anode material is driven by its concentration gradient, mechanical stress state at the current configuration, and variation of the elastic energy potential due to lithiation. Furthermore, the expression of PK-II stress tensor in silicon can be obtained as [18]

$$\boldsymbol{S} = \boldsymbol{F}_\theta^{-1}\boldsymbol{S}_e\boldsymbol{F}_\theta^{-T} \text{ with } \boldsymbol{S}_e = 2\partial\psi/\partial\boldsymbol{C}_e \tag{8}$$

It can be observed that the total stress as obtained above is a function of purely elastic stress and the diffusion induced deformation gradient.

2.3. Mechanical deformation of the current collector

Although lithium does not diffuse into the current collector, the current collector itself may be subjected to considerable mechanical deformation [1] as it is attached to the silicon thin film. Given that the current collector can be elastic as well as elasto-plastic, we need to consider an appropriate constitutive relationship for it. The present analysis accounts for possible inelastic deformation considering finite deformation kinematics through multiplicative decomposition of total deformation gradient as $\boldsymbol{F} = \boldsymbol{F}_e\boldsymbol{F}_p$. To determine the plastic component of the deformation gradient, $\boldsymbol{F}_p$, a flow rule of the form $\dot{\boldsymbol{F}}_p\boldsymbol{F}_p^{-1} = \dot{\lambda}\boldsymbol{N}_p$ is considered with the flow direction $\boldsymbol{N}_p = \partial\boldsymbol{f}/\partial\boldsymbol{M}_e$, where f is the yield function and λ is the plastic parameter. In the present formulation, the yield function for isotropic linearly hardening case is assumed and is of the following type:

$$f(\boldsymbol{M}_e,\bar{\varepsilon}_p) = \sqrt{\frac{3}{2}\boldsymbol{M}_e^d : \boldsymbol{M}_e^d} - \left[\sigma_y + H\bar{\varepsilon}_p\right] = 0 \tag{9}$$

with $\boldsymbol{M}_e^d$ is the deviatoric part of the Mandel stress tensor $\boldsymbol{M}_e$. The yield stress and hardening moduli are represented as σ_y and H, respectively.

2.4. Modeling interfacial delamination

As noted earlier, interfacial delamination is a primary cause for failure of thin film based anodes. We have placed special emphasis on modeling the spontaneous crack nucleation and its propagation at the interface. Toward this end, we utilize the cohesive zone methodology [26–28] to model the delamination of interface between Si-anode and the current collector. We note that this technique is equally applicable for the adhesive failure cases that may occur at the bi-material interface. This particular technique assumes that there is a process zone ahead of the crack tip where the material degrades monotonically towards complete failure to advance the crack. A cohesive law for this zone relates the displacement jump vector $\boldsymbol{\delta}$ ahead of a crack tip to the traction $\boldsymbol{t}_c$ the material exerts to resist fracture. To obtain this law, the existence of a surface potential Φ is assumed [28]. Traction in the process zone can then be obtained as:

$$\boldsymbol{t}_c = \frac{\partial\Phi}{\partial\boldsymbol{\delta}} \tag{10}$$

We have utilized the cohesive law suggested in Ref. [27] in this article, and accordingly, fracture toughness of the interface is calculated as:

$$G_c = \int_0^\infty t_e \mathrm{d}\delta_e = e\sigma_c\delta_c \tag{11}$$

Complete delamination of the cohesive interface is considered when effective traction at the interface becomes zero. In the present study, delamination is characterized by a parameter denoted as the delamination index (DI), which is measured in terms of the characteristic opening displacement δ_c with the following conditions:

$$\mathrm{DI} = \begin{cases} \delta_e/6\delta_c & \text{if } \delta_e < 6\delta_c \\ 1, & \text{if } \delta_e \geq 6\delta_c \end{cases} \tag{12}$$

The delamination index will be enumerated on the interface between the silicon thin film anode and current collector to estimate the progress of delamination. It should be noted that during

crack closure ($\delta_n < 0$) cohesive surfaces are subjected to contact constraint. If sliding of the interface along with contact occurs, we assume high frictional resistance along the interface. We emphasize the fact that our delamination model incorporates interfacial adhesion strength through a prescription of maximum traction σ_c that can be achieved, as well as surface energy through the fracture toughness G_c. Thus it can closely mimic physical situations and simulate a wide range of interface conditions ranging from perfectly bonded ones that do not allow any delamination to very weak cases that separate easily.

3. Materials and methods

3.1. Experimental method to determine open circuit potential (OCP)

Prediction of the half-cell potential requires an accurate estimation of the open circuit voltage $U_{OCP}(\bar{x})$. However, these parameters depend on the mechanical configuration as well as the material properties of the anode. Thus we have performed GITT experiments for estimating the $U_{OCP}(\bar{x})$ for a 250 nm thick *a*-Si thin films deposited on a Cu substrate [24]. The 250 nm thick film of *a*-Si was prepared by radio frequency (RF) magnetron sputtering. The details of the deposition conditions and the fabrication of the 2016 coin cells for electrochemical testing can be found in a previous publication [5]. Prior to GITT, the half-cell was cycled at *C*/4 current rate for 5 charge/discharge cycles to ensure the formation of the (solid–electrolyte interface) SEI layer. For the GITT, galvanostatic lithiation of the fully discharged *a*-Si anode was carried out in repeated segments of 1 h at *C*/25 rate followed by a relaxation period of 10 h to ensure equilibration. The cut-off voltage was set to 0.02 V vs. Li/Li^+ electrode. Similar process for delithiation of the fully lithiated anode was carried out and the cut off voltage was set to 1.2 V vs. the Li/Li^+ electrode. The $U_{OCP}(\bar{x})$ data obtained from the GITT experiment was fitted as a function of Li intercalation coefficient ($\bar{x}$) using cubic splines (Fig. S2) and is used for all the simulations performed for this study.

3.2. Computational methods

We have developed a finite element based computational procedure to solve coupled lithium transport and mechanical equilibrium equations. Our goal is to determine the concentration of lithium $c(\boldsymbol{X},t)$ in the active material, and the resulting displacement $\boldsymbol{u}(\boldsymbol{X},t)$of the anode for a given capacity *C* and charge rate (*C*-rate). The electrochemical cycling simulation was carried out between the upper and lower limits of the voltage window for the half-cell. The duration of charge and discharge cycle was post-processed by finding the voltage change $V(t)$ across the anode and electrolyte interface. We examine the delamination of anode from the current collector by mapping $DI(\boldsymbol{X},t)$on the undeformed cohesive surface Γ_c. For efficient numerical implementation, we employ the operator split technique to solve the coupled system of equations. In the present approach, transport of lithium was solved at the first stage assuming that the domain is held fixed at its mechanical equilibrium. In the second stage, mechanical equilibrium equation was solved assuming no transport in the anode. Variational forms of the coupled equilibrium and transport equations were obtained to perform finite element semi-discretization in space. A Newton–Raphson scheme based linearization procedure was used to solve the resulting algebraic equations in an iterative manner. A backward Euler implicit time stepping algorithm was employed to solve the resulting temporal ordinary differential equations numerically. Finite element discretization of the solid domain is performed with 8-noded brick elements. The interface between the island and substrate is modeled by 8-noded cohesive elements of zero thickness.

3.3. Computational domain

The numerical model presented in the previous section has been used to simulate the electrochemical and mechanical response of the silicon thin film along with the current collector as well as the interface between them. After the first cycle of charge and discharge, *a*-Si film exhibits through-thickness cracks forming separate islands attached to the current collector (see schematics in Fig. 2(a)) [1]. After stabilization of this crack pattern, the stresses generated in the film are not sufficient to generate additional vertical cracks [29]. However, further electrochemical cycling affects mechanical integrity of the anode configuration through the propagation of interfacial cracks that may peel off the silicon island from the current collector. In this study we have focused on the delamination of a single island subjected to electrochemical cycling similar to the experimental conditions adopted by Maranchi et al. [5]. To simulate the delamination of *a*-Si thin film from the current collector, we have considered a three-dimensional domain as shown in Fig. 2(b), where the substrate represents the current collector and the island on top of substrate represents the Si thin film. Adhesion of *a*-Si thin film with the substrate is described by the fracture strength and fracture toughness of the interface that can be obtained experimentally [1]. Separation between the vertical cracks formed in the thin film during first electrochemical cycle has been observed to be in the micron range [1]. Thus we have considered a 1 μm square thin film island of 250 nm thickness for the modeling purpose. Three-fold larger dimensions were considered for the current collector so that its boundaries do not influence the stress field in and around the interface between the film and substrate. As we are considering galvanostatic charging and discharging, a constant Li-ion flux is applied through the top surface of the *a*-Si island as shown in Fig. 2(b). Taking advantage of the symmetry, we have considered only 1/4th of the domain presented in Fig. 2(c) to minimize the computational burden.

4. Simulation results

We present the results of a detailed parametric study of the effect of mechanical properties of the current collector on the delamination behavior of the thin film during electrochemical cycling. The simulation results will be presented here for a single electrochemical cycle closely mimicking half-cell experiments. Since the formation of SEI layer and associated irreversible capacity loss as well as the formation of islands due to vertical cracking of the thin film during the first electrochemical cycle are neglected in our analysis, simulations are reported for the 2nd charge/discharge cycle. Mechanical and transport properties of the system used for the simulation purpose have been listed in Table 1. Material properties for the thin film have been chosen as that of amorphous silicon with a Young's modulus of $E_a^0 = 90$ GPa in the absence of lithiation, and a Poisson's ratio of 0.28. The current collector is taken to be of elasto-plastic nature so that it can exhibit fully recoverable elastic deformation as well as permanent plastic deformation. As we are interested in the effect of mechanical properties of the current collector on the delamination response of the thin film, we have taken these properties as our simulation parameters and varied them to span the entire feasible range. We have chosen Young's modulus to characterize the elastic regime of the current collector, and varied it from 9 GPa to 120 GPa. To investigate the effect of onset of plastic flow of the current collector on interfacial delamination, we have varied its yield strength widely from 70 to 1000 MPa, while keeping the hardening parameter constant. Note that delamination of the interface critically depends on the interfacial properties which in turn depend on the quality of adhesion achieved between silicon film and current

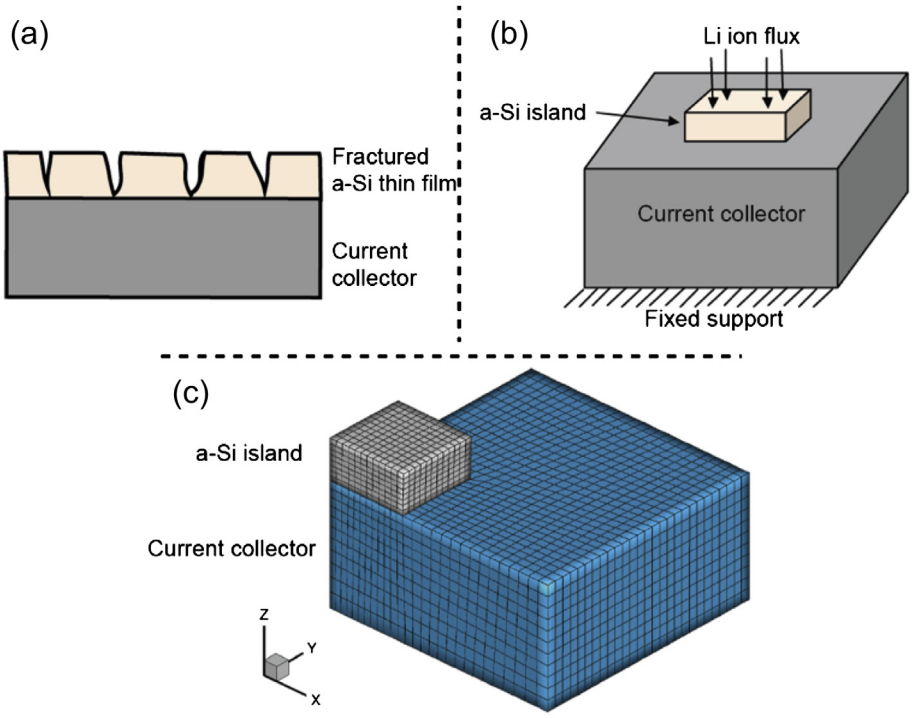

Fig. 2. (a) Vertically fractured *a*-Si thin film anode after 1st electrochemical cycle. (b) Domain representing a single *a*-Si island on the current collector with Li flux from top (c) Finite element mesh of 1/4th of the *a*-Si island and current collector domain.

collector material. However, as we are examining only the effect of substrate properties on the delamination, we keep these interfacial properties constant. We have chosen a moderately strong interface with a fracture toughness of 25 J m^{-2} as reported in Ref. [5]. The fracture strength is taken to be 2 GPa. Further details of the numerical simulation parameters are presented in Section 4 of SI.

4.1. Experimental calibration of rate constants

Reaction rate constant k to be used in the Butler–Volmer expression depends strongly on the anode configuration and experimental set up. To obtain a better estimate of this parameter, we first calibrate the simulated voltage–capacity curve for a particular charge rate against experimental results reported in literature [5]. These experiments were performed on a 250 nm *a*-Si thin film at *C*/2.5 and 2*C* charge rates. We found that $k = 1.55 \times 10^{-13}$ $m^{2.5}$ s^{-1} $mol^{-0.5}$ for lithiation and $k = 60 \times 10^{-13}$ $m^{2.5}$ s^{-1} $mol^{-0.5}$ for the corresponding delithiation appear to be in excellent agreement with the experimental values for the 0.02–1.2 V voltage window except at the onset of lithiation for *C*/2.5 charge rate. Using the same parameters, the voltage profile for 2*C* charge rate was simulated and was found to be in good agreement with the experimental results. Fig. 3 shows a comparison of the experimental and simulated voltage–capacity plots for electrochemical cycling of 250 nm thin film of *a*-Si anode at *C*/2.5 and 2*C* charge rates.

4.2. Voltage–capacity simulation at various charge rates

To further investigate the validity of the estimated parameters and demonstrate model predictive capability, calibrated model from the last section has been utilized herein to predict the

Table 1
Values of model parameters.

Parameter	Value
c_e	1000 mol m^{-3}
c_{max}	3.651×10^5 mol m^{-3}
D	10^{-16} m^2 s^{-1} [31]
E (silicon)	90 GPa
ν (silicon)	0.28
m	71.25 GPa [25]
σ_c	2 GPa
G_c	25 J m^{-2}
H	5 GPa
k (lithiation)	1.55×10^{-13} (m s^{-1})(mol m^{-3})$^{-0.5}$
k (delithiation)	60×10^{-13} (m s^{-1})(mol m^{-3})$^{-0.5}$
F	96,485.34 C mol^{-1}
R	8.314 J K^{-1} mol^{-1}
T	298 K
α_a, α_c	0.5
η	4.5×10^{-6} m^3 mol^{-1}

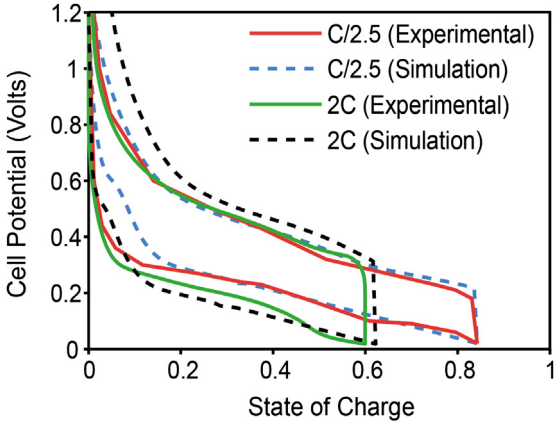

Fig. 3. Comparison of simulated and experimental voltage–capacity plots for *C*/2.5 and 2*C* charge rate.

voltage–capacity curves at different *C*-rates. Fig. 4 shows the effect of charge rates on the voltage–capacity curve. It can be observed that the electrochemical cycling at *C*/5 rate shows a higher SOC (91.6%) while only 62% SOC can be achieved with 2*C* rate. This is to be expected as lithiation is carried out in shorter duration causing higher Li flux at 2*C* rate compared to *C*/5 rate, and thus develops a comparatively higher concentration gradient inside the bulk of the thin film. This fact results in an increased over-potential due to kinetic limitations at higher charge rates and the lithiation cut-off voltage (0.02 V) is reached earlier limiting the deliverable capacity of the electrode. We further estimate maximum capacity at various charge rates and compare them with the available experimental results. Circles in the inset of Fig. 4 denote predicted values while triangles indicate the experimentally obtained ones. Maranchi et al. [5] experimentally observed an initial 2nd cycle reversible capacity of ~3500 mAh g^{-1} for the charge rate of *C*/2.5 while that for a 2*C* charge rate was ~2500 mAh g^{-1}. Our simulations predict the capacity of 3486 mAh g^{-1} for the earlier case, and 2604 mAh g^{-1} for the second one. Thus, it can be concluded that model predictions for the 2nd cycle reversible capacity agree well with the experimental results.

4.3. Mechanisms for delamination of silicon thin film from the current collector

In order to understand how the current collector deforms and possibly contributes to the delamination behavior of the interface, we first focus on two representative materials with disparate mechanical properties. The first model material is chosen to be similar to graphite, which has a low modulus of elasticity of about 9 GPa and exhibits negligible plastic deformation; and another is similar to copper, a material with Young's modulus comparable to silicon (90 GPa) but possessing yield strength of 330 MPa.

Fig. 5 shows the island and the elastic graphite substrate after completion of lithiation (Fig. 5(a)) and delithiation (Fig. 5(b)). Note that the thin film undergoes considerable deformation in the lateral directions during lithiation. Also, as the edges as well as the top of the island are free, the film bends in a convex upward manner and consequently deforms the current collector. However, as the substrate is very soft, it also deforms elastically to follow the island, and thus the interfacial displacement jump is minimal. Insets in the figure show the contours of DI, the normalized effective displacement jump. Note that maximum value of DI does not exceed 0.07. As a consequence, the interface remains intact and does not show

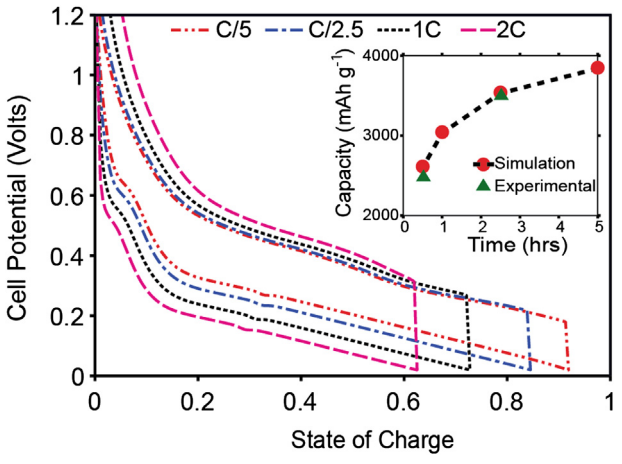

Fig. 4. Comparison of *a*-Si anode half cell potential vs. SOC at different charge rates. Inset compares the simulated and experimental capacities at different charge rates.

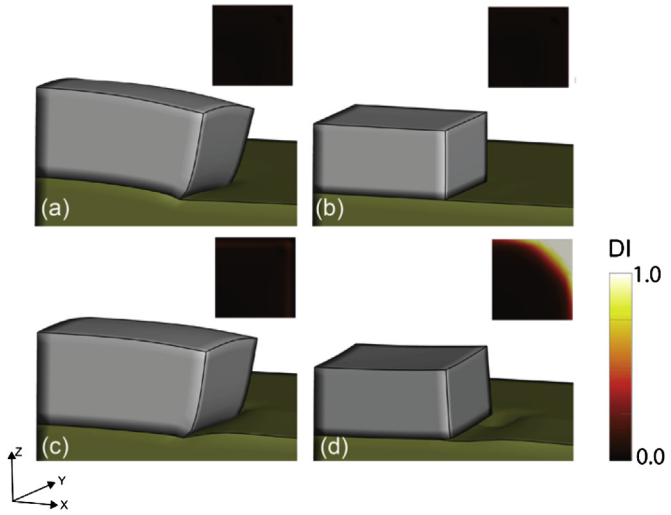

Fig. 5. Silicon island and graphite current collector at the (a) end of lithiation and (b) end of delithiation. Silicon island and copper current collector at the (c) end of lithiation and (d) end of delithiation. The contour plot in inset of each figure shows the delamination index (DI) mapped on the silicon film–current collector interface.

any delamination. During delithiation the thin film as well as the current collector recover elastically and go back to their original configuration. The stress state in the system follows a reverse chronological path as compared to lithiation, and thus does not exhibit any delamination in this phase of the electrochemical cycling.

The mechanical state for the elasto-plastic substrate with properties similar to copper is completely different. Deformation patterns for the island after completion of lithiation as well as delithiation are shown in Fig. 5(c) and (d), respectively. Note that, in contrast to the previous figure, clear delamination can be observed for this case at the end of delithiation. The delamination starts at the corner of the island during delithiation and subsequently propagates toward the center. For the elasto-plastic substrate, stresses in the vicinity of the *a*-Si island base reaches its yield strength rather early during lithiation. Therefore, considerable plastic flow of copper occurs and continues till the end of lithiation. During de-lithiation, elastic recovery of the current collector is initiated albeit substantially lower in magnitude compared to the permanent plastic deformation already achieved. Therefore, the copper substrate retains the indentation mark at the edges of the island where the plastic deformation is maximum, see Fig. 5(d). Such observation has been reported experimentally [8]. We show the contours of plastic strain on the current collector surface at the end of lithiation as well as delithiation in Fig. 10(d) and (e), respectively. These figures also reinforce our observation that considerable inelastic deformation occurs in the current collector during electrochemical cycling. Fig. 6 shows the evolution of DI during delithiation along a straight line from the center to the corner of the island. The normalized distance along this straight line is 0 for the center and 1 for the corner, respectively. This figure clearly shows that while interfacial displacement jump is minimal at the start of delithiation, it increases rapidly to the state of complete delamination (DI = 1) at the corner of the island after about 2/3rd of the delithiation phase. After its initiation, the delamination front propagates rapidly from the corner toward the center of the interface throughout the rest of the delithiation process.

It can be concluded from the above discussion that properties of the current collector exert a profound effect on the mechanical integrity of the interface. In the following sections, we study these effects in further detail.

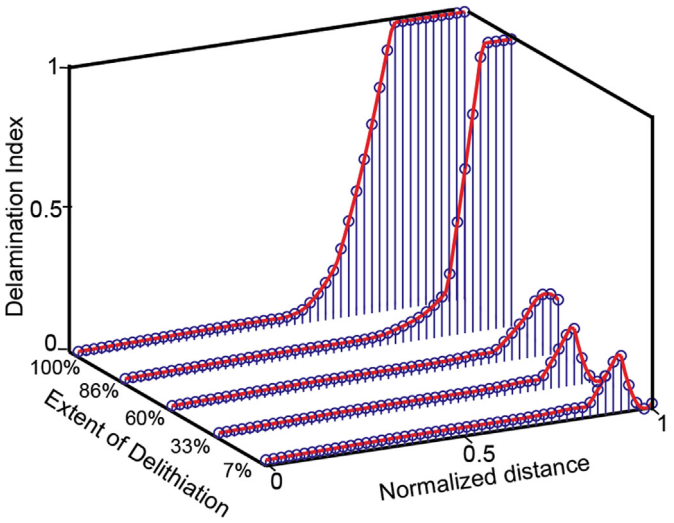

Fig. 6. Propagation of delamination front along normalized distance from the center (indicated as 0) to the corner (indicated as 1) of the island–current collector interface at different extent of delithiation.

4.4. Effect of elastic modulus of current collector on the delamination of the interface

First we focus on the effect of elastic deformation of the current collector on the interfacial delamination. So, we consider the current collectors that can undergo only elastic deformation but no plastic deformation. We vary the elastic modulus of the substrate from 9 GPa to 120 GPa keeping the film elastic modulus constant at 90 GPa. Extent of the delamination of the interface as a percentage of the entire interfacial area has been recorded and is shown in Fig. 7 for different substrate moduli. It is interesting to note that while cases with low current collector elastic modulus do not show any delamination at all, those with moduli greater than 1/3rd of that of the film undergo complete delamination. We found that delamination initiates during lithiation phase, and propagates through the entire interface readily after initiation. As discussed in the last section, soft substrates (<30 GPa) can undergo very large deformation and thus interfacial stresses may not exceed the adhesion strength of the interface. However, the mechanical situation is different for stiffer current collectors. They produce higher stresses at the interfacial region and once the crack is nucleated it is driven through the entire interface, as no other energy dissipating mechanism is present. Thus, while soft elastic substrates (<30 GPa) can prevent the onset of delamination, the situation differs entirely for elastic substrates with moderate to high stiffness: Delamination is catastrophic for these cases resulting in complete loss of electrochemical capacity.

4.5. Effect of yield strength of the current collector on the delamination of the interface

We now turn out attention to the case of elasto-plastic substrate materials and vary the yield strength from 70 MPa to 1000 MPa. We have chosen three particular instances of modulus, one with a low value of $E = 18$ GPa denoted as case 1, and other two with 60 and 90 GPa marked as cases 2 and 3, respectively. Interestingly, the soft substrate material of case 1 that did not exhibit any delamination in the absence of inelastic deformation mechanisms, can now show considerable delamination (in excess of 10%) depending on its yield strength (Fig. 8). The extent of delamination decreases rapidly with increasing yield strength and effectively vanishes for simulation materials with yield strength in excess of 1 GPa. However, substrates in cases 2 and 3 that exhibited complete delamination of the island during elastic only deformation mode undergo only limited delamination when plasticity is present, see Fig. 8. Thus, inelastic deformation mechanisms have opposing effects on the substrate materials that resided on complete delamination or no delamination regime as found from purely elastic analysis (Fig. 7). Plasticity limited the extent of delamination for the class of materials with an elastic modulus of >30 GPa while introducing delamination for the softer ones (<30 GPa elastic modulus).

We further explore these findings by performing a parametric study on the extent of delamination by varying the elastic modulus of the current collector from 18 GPa to 120 GPa. We have chosen three instances of yield strength value from its feasible range and have presented the results in Fig. 9. Note from this figure that for

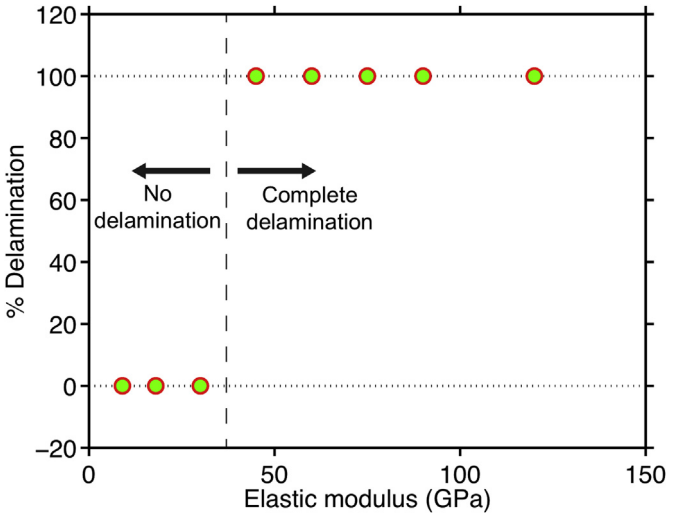

Fig. 7. Percentage of delamination for different Young's moduli of an elastic substrate. Regime of no delamination and complete delamination regime are approximately marked by the vertical dashed line.

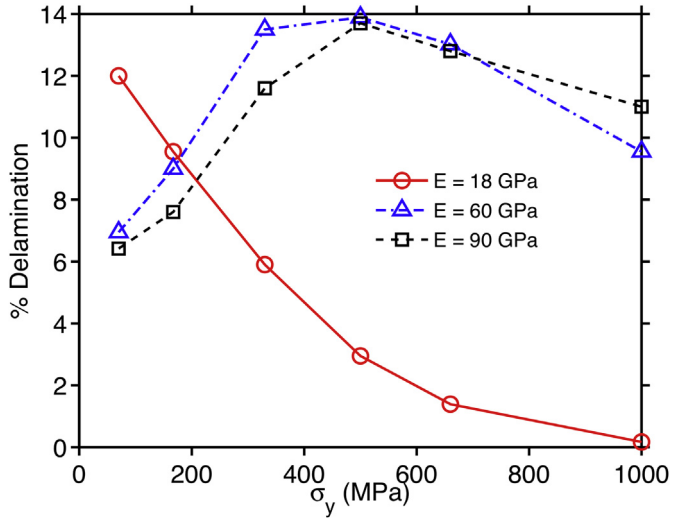

Fig. 8. Variation of percentage of delamination at island–current collector interface with yield strength of elasto-plastic current collector. Simulations have been performed for three different elastic moduli of the current collector and are indicated by separate lines (18 GPa: solid line, 60 GPa: dash-dot line and 90 GPa: dashed line).

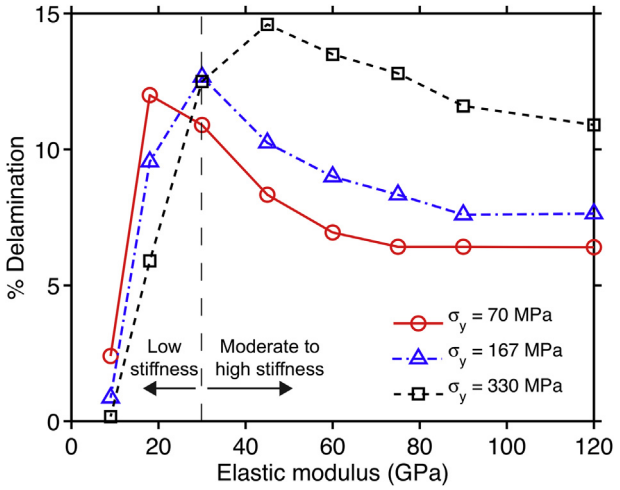

Fig. 9. Variation of percentage of delamination at island–current collector interface with Young's moduli of the elasto-plastic current collector. Simulations have been performed for three different yield strengths of the current collector and are indicated by separate lines (70 MPa: solid line, 167 MPa: dash-dot line, 330 MPa: dashed line).

softer substrates (<30 GPa), an increase in yield strength decreases the extent of delamination while opposite is true for substrates with higher modulus reinforcing our earlier observation. For all three cases of yield strength considered, the extent of delamination initially increases to reach a peak value as the elastic modulus is increased. A further increase in the modulus reduces the extent of delamination.

A detailed study of the stress state and accumulated plastic strain in the substrate materials was undertaken to elucidate the observed extent of interfacial delamination presented above. In general, there are two competing energy dissipating mechanisms occurring at and in the vicinity of the interface: permanent deformation due to plastic flow of the current collector, and creation of new surface due to delamination of the interface. During lithiation, stress state in the vicinity of the island corner remains compressive and shear dominant while during delithiation it becomes tensile and shear dominant. For the range of material properties studied, stress in the substrate typically exceeds the yield strength during lithiation. Plastic deformation of the current collector thus can be observed around the corner of the island for all cases. During delithiation, a complex interplay between these two competing mechanisms takes place that determines the ultimate extent of delamination at the interface.

The results of our study are summarized in Fig. 10. We choose a current collector material with the same elastic modulus as silicon (90 GPa), and another soft material with a modulus of 18 GPa. Three different values of yield strength are taken for each of them thus resulting in six distinct material property combinations as presented in the rows of the figure. First two columns in this figure correspond to accumulated plastic strain in the current collector in the vicinity of the island at the end of lithiation (left) and delithiation (center), respectively, while the right column represents the extent of delamination of the island–current collector interface. Observe that the stiffer material (top three rows) undergoes plastic deformation that allows it not to delaminate during lithiation as would be the case for the pure elastic case with same stiffness. It undergoes further plastic straining during delithiation relieving the stress around the interface. However, extent of this mode of deformation decreases as the yield strength is increased. As a consequence, the extent of interfacial delamination shows an increasing trend as the yield strength is increased.

The substrate material with low stiffness value (bottom three rows) can undergo very high elastic deformation and thus can keep

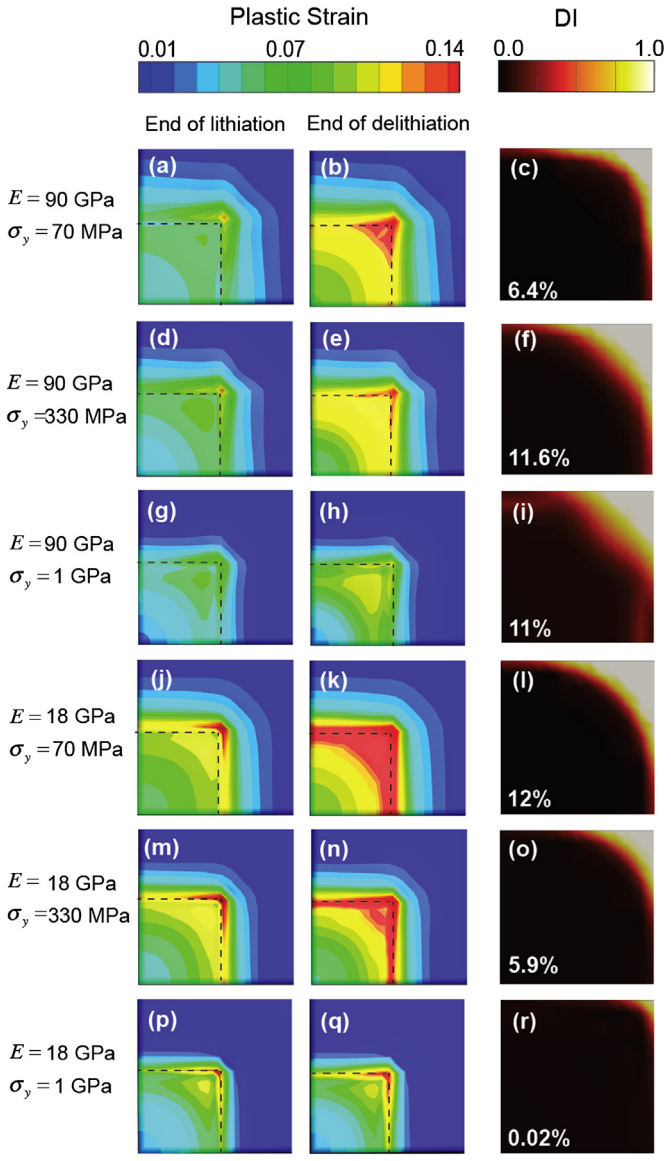

Fig. 10. Contour plot of plastic deformation at the top surface of elasto-plastic current collector at the end of lithiation (Column 1) and the end of delithiation (Column 2). Dashed lines on the current collector top surface indicate the reference position of the island. The delamination index for corresponding Si island–current collector interface is shown in Column 3. Percentage of delaminated area is also indicated.

the interfacial stresses low throughout the electrochemical cycle. However, their elastic recovery during delithiation is hindered in the presence of plasticity thus channeling the stored elastic energy toward dissipating mechanisms. Lower yield stress in these materials increases the extent of plastic deformation during lithiation thus making elastic recovery during delithiation more difficult. As a consequence, the extent of delamination increases with the yield stress.

5. Discussion

In this paper, we report the effect of the mechanical properties of the current collector on the interfacial delamination of silicon thin film based anodes. A novel multiphysics model taking into account lithium transport in the silicon anode and associated stress generation combined with the possible mechanical failure was developed. We have calibrated the model parameters and then

validated it against voltage–capacity results obtained from half-cell experiments conducted on anodes of similar configuration. The simulated voltage–capacity curve was compared against the experimental results in Fig. 3. A sudden drop in voltage at the onset of lithiation in the experimental data indicates that a higher over-potential was encountered. Presence of higher over-potential than that predicted by our model in this range indicates a loss of energy due to mechanisms that are not considered in our model, such as stress-potential coupling that is present in the physical configuration. We also have not considered the presence of SEI layer on the thin film and the expected side reactions known to occur during lithiation. These facts may explain the discrepancy of our simulation results with the experiments at the early stage of lithiation. Apart from this, the model prediction is in excellent agreement with the experimental results.

Once calibrated, the model can be used for voltage–capacity simulation at different charge rates and to estimate the maximum reversible charge capacity available. We have demonstrated the predictive capability of the model by simulating the voltage–capacity curve for different charge rates. Our model predicts the experimental charge capacity of the anode subjected to different *C*-rates with reasonable accuracy. The model is also capable of simulating consecutive electrochemical cycling experiments with the evolution of voltage–capacity curve and the mechanical configuration dependent stresses. Often, experimentalists vary the voltage window in which the anode half cell is cycled for various reasons, in particular, to reduce the volumetric expansion, etc. The capacity obtained at various cut off potentials can also be estimated by this model.

The modeling framework was next utilized to predict the crack propagation at the interface between *a*-Si thin film and current collector. Although studies on delamination mechanisms of silicon thin films have been reported recently in the literature [8,13,14], the influence of current collector mechanical properties on this phenomenon has not received much attention. A recent experiment has demonstrated that a layer of carbon placed between the film and copper current collector extends the cyclic life of the thin film anode substantially [15]. This fact, along with the observation reported in literature [1] that the film completely delaminates after a few cycles from the copper substrate, has motivated us to study the effect of substrate mechanical properties in detail.

While the experimental studies mentioned above provide valuable insight into the various mechanisms responsible for *a*-Si thin film anode performance, detailed knowledge of the relationship between these physico-chemical phenomena and the perceived ultimate failure of the anode is still lacking. Computational models as discussed in this article are thus valuable in understanding the role of various contributing mechanisms and their mutual interaction toward electrode performance. This knowledge base will help determine the experimental parameters required for achieving the desired design objective of a fully functional silicon anode.

Our simulations reveal that the elastic modulus as well as extent of inelastic deformation of the current collector are important design parameters that influence the mechanical stability of the anode configuration. An elastic substrate with low elastic modulus is the best design option to safe guard against interfacial delamination. Recent experiments with soft elastic current collectors such as graphite [15] and polymers [9] have shown excellent electrochemical cycling performance. While not mentioned explicitly in these reports, our analysis suggests that the mechanical stability stemmed from the choice of substrate materials properties itself. If a material with higher stiffness has to be chosen, it is better to consider the candidates that can undergo plastic deformation. However, they will exhibit some extent of delamination that may eventually extend through the entire interface in the course of further electrochemical cycling.

Separation between the current collector and active material can increase the contact resistance leading to an Ohmic drop and resultant reduction in capacity. Although contact resistance increment is negligible for the amount of delamination shown in the simulations, it can increase exponentially as the interfacial debonding progresses over many cycles. It can be conjectured that some irreversible mechanisms operate during electrochemical cycling that can trigger the partial debonding of *a*-Si film leading to complete catastrophic failure. In the present study, we assume interfacial parameters such as fracture energy and strength to be constant. A cycle-wise reduction of these parameters may lead to catastrophic debonding of the *a*-Si island as observed experimentally [1]. The dislocation pile up in the substrate due to plastic flow [30], precipitation of lithium atoms in the interfacial region and subsequent trapping, and migration of copper atoms in the interface [1] may all lead to an altered state at the interface that may change interfacial failure properties irreversibly. Relevant irreversible mechanisms are also expected to operate at the interfacial region for the cases with elastic substrate with low modulus. However, their effect is expected to be significantly low considering that interfacial crack has not nucleated yet. Therefore, a soft elastic substrate can promise good capacity retention for a large number of electrochemical cycles. Indeed, Yu et al. [9] have demonstrated excellent capacity retention of 84.6% after 500 cycles using microfabricated ribbons of Si thin film (100–400 nm) and (70–200 μm wide) on poly(dimethylsiloxane) (PDMS) substrate. PDMS, being a very low modulus elastic material, further supports our above-mentioned observation. It is therefore envisaged that these computational mechanics based models will help the experimentalists design improved silicon based anode systems.

6. Conclusions

Novel multi-physics computational methodology has been developed that couples electrochemical processes with finite elasticity based modeling to predict voltage–capacity behavior of the half-cell as well as its mechanical degradation. Reasonable agreement has been observed between the capacities predicted by simulation and those determined experimentally. Indubitable profound influence of the mechanical properties of the substrate including the yield strength and elastic modulus on the stress assisted delamination has been predicted providing a good rationale for designing future thin film based anode systems.

Acknowledgments

The authors would like to acknowledge the financial support from the US Department Of Energy's Office Of Vehicle Technologies BATT Program (Contract DE-AC02-05CHI1231), sub contract 6151369, and the National Science Foundation (CBET-0933141). PNK would also like to acknowledge the Edward R. Weidlein Chair Professorship Funds for partial support of this work. In addition, PNK and SM would like to thank the Center for Complex Engineered Multifunctional Materials (CCEMM) for providing a graduate fellowship to perform the simulations and experiments reported in this work.

Appendix A. Supplementary data

Supplementary data related to this article can be found at http://dx.doi.org/10.1016/j.jpowsour.2013.06.089.

Nomenclature

c	concentration of Li in the reference configuration (mol m^{-3})
c_e	Li concentration in electrolyte (mol m^{-3})
c_{max}	maximum lithiation concentration in anode material (mol m^{-3})
c_s	concentration of Li on the surface of the active material (mol m^{-3})
C	capacity of the electrode material (mAh g^{-1})
$\boldsymbol{C}$	Cauchy-Green tensor
C-rate	charge rate
D	diffusivity of Li atom in the anode material (m^2 s^{-1})
DI	damage index
E	Young's modulus (Pa)
f	yield function
F	Faraday's constant (C mol^{-1})
$\boldsymbol{F}$	deformation gradient
$\boldsymbol{F}_e$	elastic component of the deformation gradient
$\boldsymbol{F}_\theta$	expansion component of the deformation gradient
G_c	fracture toughness of the interface (J m^{-2})
H	hardening modulus (Pa)
i_0	exchange current density (A m^{-2})
I	constant current applied to the electrode during galvanostatic simulations (A)
$\boldsymbol{J}$	Li atom flux (mol m^{-2} s^{-1})
k	kinetic rate constant (m s^{-1})(mol m^{-3})$^{-0.5}$
m	rate of change of elastic modulus of a-Si with Li fraction (Pa $Li^{-1}_{fraction}$)
$\boldsymbol{M}_e$	Mendel stress tensor
$\boldsymbol{P}$	first Piola–Kirchhoff stress tensor
R	universal gas constant (J K^{-1} mol^{-1})
R_c	contact resistance between current collector and electrode material (Ω m^2)
$\boldsymbol{S}$	second Piola–Kirchhoff stress tensor
$\boldsymbol{t}$	applied traction vector
$\boldsymbol{t}_c$	traction at the cohesive surface
t_e	effective traction
T	temperature (K)
$\boldsymbol{u}$	displacement field
$U_{OCP}(\bar{x})$	Li intercalation coefficient dependent open circuit voltage of Li–Si electrode vs. Li/Li^+ ref. (V)
$\boldsymbol{x}$	position vector of material point in current configuration
$\bar{x}$	Li intercalation coefficient
$\boldsymbol{X}$	position vector of material point in reference configuration
α_a, α_c	anodic and cathodic transfer coefficient
$\boldsymbol{\delta}$	displacement jump vector
δ_e, δ_c	effective and characteristic opening displacement jump
ϕ	deformation map
Φ	cohesive potential
η	coefficient of expansion (m^3 mol^{-1})
η_s	overpotential (V)
μ	chemical potential in the reference configuration
ν	Poisson's ratio
σ_c	maximum cohesive normal traction
σ_y	yield strength of the material (Pa)
Ω_0	reference configuration
Ω_t	spatial configuration
ψ	free energy functional

References

[1] J.P. Maranchi, A.F. Hepp, A.G. Evans, N.T. Nuhfer, P.N. Kumta, Journal of The Electrochemical Society 153 (2006) A1246.
[2] U. Kasavajjula, C. Wang, A.J. Appleby, Journal of Power Sources 163 (2007) 1003–1039.
[3] B. Scrosati, J. Garche, Journal of Power Sources 195 (2010) 2419–2430.
[4] W.-J. Zhang, Journal of Power Sources 196 (2011) 13–24.
[5] J.P. Maranchi, A.F. Hepp, P.N. Kumta, Electrochemical and Solid State Letters 6 (2003) A198.
[6] C.C. Nguyen, S.-W. Song, Electrochimica Acta 55 (2010) 3026–3033.
[7] L.B. Chen, J.Y. Xie, H.C. Yu, T.H. Wang, Journal of Applied Electrochemistry 39 (2009) 1157–1162.
[8] X. Xiao, P. Liu, M.W. Verbrugge, H. Haftbaradaran, H. Gao, Journal of Power Sources 196 (2011) 1409–1416.
[9] C. Yu, X. Li, T. Ma, J. Rong, R. Zhang, J. Shaffer, Y. An, Q. Liu, B. Wei, H. Jiang, Advanced Energy Materials 2 (2012) 68–73.
[10] G. Cho, J. Noh, H. Sung, S. Choi, S. Lee, H. Ahn, T. Nam, K. Kim, Microelectronic Engineering 89 (2012) 104–108.
[11] S. Soni, B.W. Sheldon, X. Xiao, M.W. Verbrugge, A. Dongjoon, H. Haftbaradaran, H. Gao, Journal of The Electrochemical Society 159 (2011) A38–A43.
[12] H. Haftbaradaran, H. Gao, Applied Physics Letters 100 (2012) 121907-1–121907-4.
[13] H. Haftbaradaran, S.K. Soni, B.W. Sheldon, X. Xiao, H. Gao, Journal of Applied Mechanics 79 (2012) 031018-1–031018-6.
[14] H. Haftbaradaran, X. Xio, M.W. Verbrugge, H. Gao, Journal of Power Sources 206 (2012) 357–366.
[15] M.K. Datta, J. Maranchi, S.J. Chung, R. Epur, K. Kadakia, P. Jampani, P.N. Kumta, Electrochimica Acta 56 (2011) 4717–4723.
[16] Z. Cui, F. Gao, J. Qu, Journal of the Mechanics and Physics of Solids 60 (2012) 16.
[17] A.F. Bower, P.R. Guduru, Modelling and Simulation in Materials Science and Engineering 20 (2012) 20.
[18] S. Pal, S. Damle, S. Patel, M.K. Dutta, P.N. Kumta, S. Maiti, ECS Transactions 41 (2012) 87–89.
[19] K. Zhao, M. Pharr, J.J. Vlassak, Z. Suo, Journal of Applied Physics 109 (2011) 016110.
[20] A.F. Bower, P.R. Guduru, V.A. Sethuraman, Journal of the Mechanics and Physics of Solids 59 (2011) 804–828.
[21] R. Grantab, V.B. Shenoy, Journal of The Electrochemical Society 8 (2011) A948–A954.
[22] R. Grantab, V.B. Shenoy, Journal of The Electrochemical Society 5 (2012) A584–a591.
[23] J.O. Bockris, A.K.N. Reddy, M. Gamboa-Aldeco, Modern Electrochemistry 2A: Fundamentals of Electrodics, Springer, 2001.
[24] L. Baggetto, J.F.M. Oudenhoven, T. van Dongen, J.H. Klootwijk, M. Mulder, R.A.H. Niessen, M.H.J.M. de Croon, P.H.L. Notten, Journal of Power Sources 189 (2009) 402–410.
[25] V.B. Shenoy, P. Johari, Y. Qi, Journal of Power Sources 195 (2010) 6825–6830.
[26] S. Maiti, P. Geubelle, Engineering Fracture Mechanics 73 (2006) 22–41.
[27] M. Ortiz, A. Pandolfi, International Journal for Numerical Methods in Engineering 44 (1999) 1267–1282.
[28] K. Park, G.H. Paulino, J.R. Roesler, Journal of the Mechanics and Physics of Solids 57 (2009) 891–908.
[29] J. Li, A.K. Dozier, Y. Li, F. Yang, Y.-T. Cheng, Journal of The Electrochemical Society 158 (2011) A689.
[30] V.S. Deshpande, A. Needleman, E. Van der Giessen, Acta Materialia 51 (2003) 15.
[31] R. Chandrasekaran, T.F. Fuller, Journal of The Electrochemical Society 158 (8) (2011) A859.